Text S1 Materials and methods

For N-DOM, 10 mg NOM sample was added into 500 mL ultrapure water, the derivation experiments were conducted in the same conditions.

The experimental data of DOC during the derivation processes of MPs-DOM and N-DOM were fit by the kinetic models listed in Table S1.

Table S1 Kinetic models.

Kinetic models	
Zero-order	$C_t = k_0 t$
First-order	$C_t = C_0 e^{-k1t}$
Second-order	$1/C_t = 1/C_0 + k_2 t$
Intraparticle diffusion	$C_t/C_{max} = k_p t^{0.5} + S$
Boyd film diffusion	$B_t = -\ln(1 - C_t/C_{max}) - 0.4977$

C_t: leached DOC concentration at time t, mg-C/L; C_0: initial DOC concentration, mg-C/L; k_0: zero-level kinetic rate constant, mg/(g·h); *t*: reaction time, h; k_1: first-level kinetic rate constant, h^{-1}; C_{max}: maximum leached DOC concentration, mg-C/L; k_2: second-level kinetic rate constant, g/(mg·h) ; k_p: intraparticle diffusion model rate constant, (mg·h)/g; S: intraparticle diffusion model constant, mg/g.

PARAFAC modeling was performed using MATLAB 2022 (Mathworks, Natick, MA, USA) and the drEEM toolbox[1]. Modeling was performed by parallel factor analysis (PARAFAC) using the DOMFluor toolbox, which uses an alternating least squares process to minimize the error term between the measured and modeled EEMs, constructed from the loadings of the three factors corresponding to excitation wavelength, emission wavelength, and fluorescence intensity.

The MPs-DOM sample and the N-DOM sample are filtered through a pre-ashed Whatman GF/F filter membrane to remove large solid impurities. Then, the water sample is acidified with hydrochloric acid and added dropwise until the pH value is 2. Extract using a solid-phase extraction column (model: Agilent Bond Elut PPL, 1.0 g, 6 mL), then dry with N_2 airflow, wash the extraction column with 1 - 2 column volumes of methanol.

Intensity-weighted average parameters (wa) of molecular formulae were calculated using Equation (10) for each spectrum. The intensity-weighted average values of O/C_{wa}, H/C_{wa} and N/C_{wa} were calculated using algorithms.

$$RI = \frac{I_i}{\sum I_i} \quad (10)$$

Double bond equivalents (DBE) were calculated to evaluate the unsaturation of

specific molecules using Equation (11). Double bond equivalent minus oxygen per carbon ((DBE-O)/C) and nominal oxidation state of carbon (NOSC) are indexes that can be used to characterize the unsaturation and oxidized states, respectively, where larger positive values suggest a higher degree of unsaturation and oxidized state. Based on these two indexes, the molecules can be divided into four states: (1) saturated and reduced ((DBE-O)/C = -0.8 - 0, NOSC = -1.5 - 0), (2) saturated and oxidized((DBE-O)/C =-0.8 - 0, NOSC = 0 - 1.5), (3) unsaturated and reduced ((DBE-O)/C = 0 - 0.8, NOSC = -1.5 - 0), (4) unsaturated and oxidized ((DBE-O)/C = 0 - 0.8, NOSC = 0 - 1.5).

$$DBE_{wa}=\sum\frac{2C+N+P-H+2}{2}\times RI_i \quad (11)$$

$$(DBE\text{-}O)/C_{wa}=\sum((DBE\text{-}O)/C_i\times RI_i)) \quad (12)$$

$$NOSC=\frac{\sum NOSC\times RI_i}{\sum RIi} \quad (13)$$

The modified aromaticity index (AI_{mod}) was used to evaluate the fraction of aromatic and condensed aromatic structures, which was calculated using Equation (14)[2].

$$AI_{mod}=\frac{1+C-0.5O-S-0.5(N+P+H)}{C-0.5O-N-S-P} \quad (14)$$

Table S2 Classification according to the degree of unsaturation of oxygen-containing functional groups and carbon skeletons.

	Criterion	
Group 1	(DBE-O)/C $\geqslant$ 0) and NOSC > 0	Unsaturated and oxidized compounds
Group 2	(DBE-O)/C > 0) and NOSC $\leqslant$ 0	Unsaturated and reduced compounds
Group 3	(DBE-O)/C $\leqslant$ 0) and NOSC < 0	Saturated and reduced compounds
Group 4	(DBE-O)/C < 0) and NOSC $\geqslant$ 0	Saturated and oxidized compounds

Table S3 Characteristics of compound classes used for categorizing FT-ICR-MS molecular formulas[3].

Compound class	Abbreviation/Name	Criterion
Condensed aromatic structure	CAS	0.2≤H/C≤0.7 0≤O/C≤0.67
Lignin/CRAM	Lignin	0.7≤H/C≤1.5 0.1≤O/C≤0.67
Protein	Protein	1.5≤H/C≤2.2 0.3≤O/C≤0.67
Carbohydrate	HydroC	1.5≤H/C≤2.4 0.67≤O/C≤1.2
Lipid	Lipid	1.5≤H/C≤2.0 0≤O/C≤0.3
Unsaturated hydrocarbon	UnsatHydroC	0.7≤H/C≤1.5 0≤O/C≤0.1
Tannin	Tannin	0.5≤H/C≤1.5 0.65≤O/C≤1

The high-performance liquid chromatography-mass spectrometry (HPLC-MS) system (Vanquish and Thermo Scientific Orbitrap Exploris 120) was used to identify the additives in plastics. A volume of 5 μL was injected onto a C18 column (2.1 × 100 mm, 1.9 μm) maintained at 35 ℃ at a flow rate of 0.3 mL/min, and the mobile phase consisted of a gradient of solvents, with water:methanol being 95:5 at 0 - 5 min, 80:20 at 5.5 - 7 min, 60:40 at 8 - 10 min, 40:60 at 11 - 15 min The scan was 20:80 at 16 - 18 minutes and 95:5 at 19 - 25 minutes, tested in negative ion mode with a scanning range of *m/z*: 50 - 1500 amu.

The experimental data were fitted by kinetic models with the linear least-squares method and multivariate statistical analysis of spectral indices using OriginPro 2021 (OriginLab, Northampton, MA, USA). One-way analysis of variance (ANOVA) was performed using SPSS 25.0 (IBM Corporation, Armonk, NY, USA) to determine the significance of the parameters using Duncan's multiple range test with a threshold of $p < 0.05$. All the data were exhibited as means ± standard deviation (SD) derived from the triple replicates.

References

[1] Murphy KR, Stedmon CA, Graeber D, Bro R. 2013. Fluorescence spectroscopy and multi-way techniques. *PARAFAC. Analytical Methods* 5(23): 6557-6566 https:// doi.org/10.1039/c3ay41160e

[2] Zeng Y, Fang G, Fu Q, Dionysiou DD, Wang X, et al. 2021. Photochemical characterization of paddy water during rice cultivation: Formation of reactive intermediates for As(III) oxidation. *Water Research* 206: 117721 https://doi.org/ 10.1016/j.watres.2021.117721

[3] Lee YK, He W, Guo H, Karanfil T, Hur J. 2023. Effects of organic additives on spectroscopic and molecular-level features of photo-induced dissolved organic matter from microplastics. Water Research 242: 120272 https://doi.org/10.1016/ j.watres. 2023.120272

Table S4 Kinetic parameters for MPs-DOM and N-DOM leaching.

Treatment			PE-DOM	PET-DOM	PBAT-DOM	PLA-DOM	N-DOM
Zero-order	Dark	k_0（mg/(g·h)）	0.002	0.001	0.001	0.005	1.330
		R^2	0.810	0.752	0.963	0.947	0.926
	UV	k_0（mg/(g·h)）	0.063	0.022	0.463	0.495	4.890
		R^2	0.917	0.833	0.990	0.987	0.751
First-order	Dark	k_1（h^{-1}）	-	0.211	-	0.427	-
		R^2	-	0.324	-	0.442	-
	UV	k_1（h^{-1}）	0.041	0.033	-	-	0.117
		R^2	0.951	0.962	-	-	0.957
Second-order	Dark	k_2（g/(mg·h)）	2.962	2.446	1.080	1.073	0.001
		R^2	0.950	0.996	0.881	0.999	0.991
	UV	k_2（g/(mg·h)）	0.266	0.099	0.006	0.008	0.002
		R^2	0.907	0.981	0.351	0.223	0.999
Intraparticle diffusion	Dark	k_{p1}	0.138	0.118	0.011	0.011	0.114
		S_1	-0.276	-0.090	0.035	0.006	0.197
		R^2	0.943	0.933	0.883	0.779	0.982
		k_{p2}	0.046	0.078	0.067	0.048	0.019
		S_2	0.172	0.048	-0.250	-0.191	0.691
		R^2	0.995	0.996	0.979	0.998	0.948

	UV	k_{p1}（(mg·h)/g）	0.063	-0.003	0.022	0.019	0.025
		S_1（mg/g）	0.434	0.901	0.333	0.839	0.700
		R^2	0.997	0.978	0.847	0.991	0.993
		k_{p2}（(mg·h)/g）	0.105	0.020	0.132	0.016	0.053
		S_2（mg/g）	-0.041	0.772	-0.382	0.839	0.448
		R^2	0.873	0.807	0.979	0.875	0.967
Boyd film diffusion	Dark	k	0.025	0.037	0.016	0.066	0.002
		S	0	0	0	0	0.752
		R^2	0.933	0.823	0.826	0.894	0.962
	UV	k	0.010	0.014	0.005	0.003	0.004
		S	-0.357	-0.299	0.562	-0.498	0.562
		R^2	0.904	0.980	0.979	0.988	0.751

Table S5 The linear fitting results between DOC_{UV}/DOC_{dark} and derivation time

	Slope	Intercept	R^2
PE-DOM	0.056	3.190	0.494
PET-DOM	0.147	7.340	0.860
PBAT-DOM	0.526	4.229	0.986
PLA-DOM	0.472	14.958	0.896
N-DOM	0.005	1.499	0.409

Table S6 Characteristic peaks of FT-IR spectrum of MPs-DOM and N-DOM.

	Wavenumber (cm^{-1})	Assignment	Ref.
PE-DOM	663#	Stretching of C-C.	(Wolpert and Hellwig, 2006)
	710#	Rocking of -CH_2.	
	1066#	Stretching of C-O.	(Salavagione et al., 2005)
	1265*	Stretching of C-O in -COOH.	(Salavagione et al., 2005)
	1328*#	Bending of -OH in phenols.	(Wolpert and Hellwig, 2006)
	1402	Symmetric stretching of COO^-; Bending of -OH in -COOH.	(Osman and Arof, 2003)
	1442*#	Stretching of C=C in aromatics; Asymmetric stretching of -CH_3; Stretching of -CH_2.	(Osman and Arof, 2003)
	1497#	Stretching of C=C in aromatics and/or quinone ring; Bending of C-H.	(Li et al., 2014)
	1550#	Symmetric stretching of -COO^-.	(Li et al., 2014)
	1630	Stretching of C=O in unsaturated aliphatics.	(Liu et al., 2006)
	1700	Stretching of C=O in aromatic carboxylic acids and/or ketone.	(Krysa et al., 2022)
	1751	Stretching of C=O in carboxylic acids and/or esters.	(Subramanian et al., 2011)
PET-DOM	731	Rocking of -CH_2; Out-of-plane bending of C-H.	(Ge et al., 2017)
	940*#	Rocking vibrations of -CH_3; Bending vibrations of C=O.	(Gómez-Serrano et al., 1999)
	1020*#	In-plane bending of C-H in aromatics.	(Subramanian et al., 2010)
	1060	Stretching of C-O; Deformation bending of -OH in alcohols.	(Krysa et al., 2022)
	1140/1150*#	Stretching of C-O in aromatics.	(Sundaraganesan et al., 2008)
	1290*#	Stretching of C=O and/or C-O.	(Chung et al., 2004)
	1400#	In-plane bending of O-H in	(Barroso-Bogeat et

		carboxylic acids.	al., 2014)
	1510	Stretching of C=C in aromatics.	(Meng et al., 2014)
	1650	Stretching of C=O in COO^-; Stretching of C=C in aromatics.	(Meng et al., 2014)
	1690#	Stretching of C=O in aromatic carboxylic acids and/or ketone.	(Asemani and Rabbani, 2020)
	2960#	Asymmetric stretching of -C-H and $-CH_2$.	(Demyan et al., 2012)
PBAT-DOM	1090*#	Stretching of C-O in alcohols and esters.	(Liu et al., 2021b)
	1210#	Stretching of C-O in esters; Vibration of aromatic ring.	(Ahmed et al., 2018)
	1370*#	Bending of -OH; Symmetric deformation of C-H.	(Djebara et al., 2012)
	1400#	Symmetric stretching of C=O in carboxylic acids and/or easters.	(Liu et al., 2021b)
	1440#	Vibration of aromatic ring; Deformation of -CH.	(Liu et al., 2021b)
	1630	Asymmetric stretching of COO^-; Stretching of C=O.	(Liu et al., 2021b)
	1730#	Stretching of C=O.	(Liu et al., 2021b)
	2960#	Asymmetric stretching of C-H in $-CH_2$.	(Hashimoto et al., 2010)
PLA-DOM	870*#	Transverse vibration of $-CH_2-$	(Zhu et al., 2014)
	1030/1040#/1050	Symmetric stretching of C-O in alcohols or easters; Deformation of -OH in alcoholics.	(Szymanska-Chargot and Zdunek, 2013)
	1070#/1080/1100	Stretching of C-O in alcohols or easters; Stretching of C-C in aromatics.	(Soliman et al., 2013)
	1130#	In-plan bending vibrations of C-H; Rocking of $-CH_3$.	(Prabhu et al., 2011)
	1190*	Stretching of C-O.	(Chung et al., 2004)
	1400	Symmetric stretching of C=O in carboxylic acids and/or easters.	(Chung et al., 2004)
	1620	Vibration of C=O; Stretching of C=C in aromatics; Asymmetric stretching of COO^-.	(Selvaraju et al., 2012)

	1650	Stretching of C=O in amide I and/or COO^-; Stretching of C=C in aromatics and/or alkenes.	(Asemani and Rabbani, 2020)
	1750	Stretching of C=O.	(Asemani and Rabbani, 2020)
	2940#	Stretching of -CH and $-CH_3$.	(Wiercigroch et al., 2017)
	3000*	Asymmetric stretching of C-H in $-CH_3$.	(Linder et al., 2005)
N-DOM	1068	Stretching of C-O.	(Rodríguez et al., 2016)
	1204	Quinone; Stretching of C-O.	(Dikdim et al., 2019)
	1402	Symmetric stretching of COO^-; Bending of -OH in -COOH.	(Kim et al., 2006)
	1497	Stretching of C=C in aromatics and/or quinone ring.	(Kim et al., 2006)
	1550	Asymmetric stretching of COO-; Stretching of C=O in quinone and/or Amide I group.	(Jaouadi et al., 2012)
	1635	Vibration of C=C in aromatics; Stretching of C=O.	(Jaouadi et al., 2012)
	1720	Asymmetric stretching of C=O in carboxylic acids and carbonyl.	(Ifon et al., 2024)
	1734	Stretching of C=O in esters and acetyls.	(Ifon et al., 2024)

*: Newly generated characteristic peaks;

#: Characteristic peaks associated with additives in plastics.

References

[1] Wolpert M, Hellwig P. 2006. Infrared spectra and molar absorption coefficients of the 20 alpha amino acids in aqueous solutions in the spectral range from 1800 to 500 cm-1. Spectrochimica Acta Part A: Molecular and Biomolecular Spectroscopy 64(4): 987-1001 https://doi.org/10.1016/j.saa.2005.08.025

[2] Salavagione HJ, Arias-Pardilla J, Pérez JM, Vázquez JL, Morallón E, et al. 2005. Study of redox mechanism of poly(o-aminophenol) using in situ techniques: Evidence of two redox processes. Journal of Electroanalytical Chemistry 576(1): 139-145 https: //doi.org/10.1016/j.jelechem.2004.10.013

[3] Osman Z, Arof AK. 2003. FTIR studies of chitosan acetate based polymer electrolytes. Electrochimica Acta 48(8): 993-999.https://doi.org/10.1016/s 0013 -4686(02)00812-5

[4] Li JR, Sun SQ, Wang XX, Xu CH, Chen JB, et al. 2014. Differentiation of five species of Danggui raw materials by FTIR combined with 2D-COS IR. Journal of Molecular Structure 1069: 229-235 https://doi.org/10.1016/j.molstruc.2014. 03.067

[5] Liu HX, Sun SQ, Lv GH, Chan KKC. 2006. Study on Angelica and its different extracts by Fourier transform infrared spectroscopy and two-dimensional correlation IR spectroscopy. Spectrochimica Acta Part A: Molecular and Biomolecular Spectroscopy 64(2): 321-326 https://doi.org/10.1016/j.saa.2005.07. 026

[6] Krysa M, Szymanska-Chargot M, Zdunek A. 2022. FT-IR and FT-Raman fingerprints of flavonoids - A review. Food Chemistry 393: 133430 https://doi.org/10.1016/ j.foodchem.2022.133430

[7] Subramanian N, Sundaraganesan N, Dereli Ö, Türkkan E. 2011. FT-IR, FT-Raman spectra, density functional computations of the vibrational spectra and molecular conformational analysis of 2,5-di-tert-butyl-hydroquinone. Spectrochimica Acta Part A: Molecular and Biomolecular Spectroscopy 83(1): 165-174 https://doi.org/10.1016 / j.saa.2011.08.010

[8] Ge SB, Liu ZL, Li RD, Furuta Y, Peng WX. 2017. Desulphurization characteristics of bamboo charcoal from sulfur solution. Saudi Journal of Biological Sciences 24(1): 127-131 https://doi.org/10.1016/j.sjbs.2016.09.005

[9] Gómez-Serrano V, Piriz-Almeida F, Durán-Valle CJ, Pastor-Villegas J. 1999. Formation of oxygen structures by air activation.: A study by FT-IR spectroscopy. Carbon 37(10): 1517-1528 https://doi.org/10.1016/s0008-6223(99)00025-1

[10] Subramanian N, Sundaraganesan N, Jayabharathi J. 2010. Molecular structure, spectroscopic (FT-IR, FT-Raman, NMR, UV) studies and first-order molecular hyperpolarizabilities of 1,2-bis(3-methoxy-4-hydroxybenzylidene) hydrazine by density functional method. Spectrochimica Acta Part A: Molecular and Biomolecular Spectroscopy 76(2): 259-269 https://doi.org/10.1016/j.saa.2010. 03. 033

[11] Sundaraganesan N, Anand B, Meganathan C, Joshua BD. 2008. FT-IR, FT-Raman spectra and ab initio HF, DFT vibrational analysis of p-chlorobenzoic acid. Spectrochimica Acta Part A: Molecular and Biomolecular Spectroscopy 69(3): 871-879 https://doi.org/10.1016/j.saa.2007.05.051

[12] Chung C, Lee M, Choe EK. 2004. Characterization of cotton fabric scouring by FT-IR ATR spectroscopy. Carbohydrate Polymers 58(4): 417-420 https://doi.org/ 10.1016/ j.carbpol.2004.08.005

[13] Barroso-Bogeat A, Alexandre-Franco M, Fernández-González C, Gómez-Serrano V. 2014. FT-IR analysis of pyrone and chromene structures in activated carbon. Energy & Fuels 28(6): 4096-4103 https://doi.org/10.1021/ef5004733

[14] Meng YY, Yao CH, Xue S, Yang HB. 2014. Application of Fourier transform infrared (FT-IR) spectroscopy in determination of microalgal compositions. Bioresource Technology 151: 347-354 https://doi.org/10.1016/j.biortech.2013. 10.064

[15] Asemani M, Rabbani AR. 2020. Detailed FTIR spectroscopy characterization of crude oil extracted asphaltenes: Curve resolve of overlapping bands. Journal of Petroleum Science and Engineering 185: 106618 https://doi.org/10.1016/j. petrol. 2019.106618

[16] Demyan MS, Rasche F, Schulz E, Breulmann M, Müller T, et al. 2012. Use of specific peaks obtained by diffuse reflectance Fourier transform mid-infrared spectroscopy to study the composition of organic matter in a Haplic Chernozem. European Journal of Soil Science

63(2): 189-199 https://doi.org/10.1111/j. 1365- 2389.2011.01420.

[17] Liu XW, Renard C, Bureau S, Le Bourvellec C. 2021b. Revisiting the contribution of ATR-FTIR spectroscopy to characterize plant cell wall polysaccharides. Carbohydrate Polymers 262: 117935 https://doi.org/10.1016/ j.carbpol.2021.117935

[18] Ahmed A, Chaker Y, Belarbi EH, Abbas O, Chotard JN, et al. 2018. XRD and ATR/FTIR investigations of various montmorillonite clays modified by monocationic and dicationic imidazolium ionic liquids. Journal of Molecular Structure 1173: 653-664 https://doi.org/10.1016/j.molstruc.2018.07.039

[19] Djebara M, Stoquert JP, Abdesselam M, Muller D, Chami AC. 2012. FTIR analysis of polyethylene terephthalate irradiated by MeV He+. Nuclear Instruments and Methods in Physics Research, Section B: Beam Interactions with Materials and Atoms 274: 70-77 https://doi.org/10.1016/j.nimb.2011.11.022

[20] Hashimoto K, Choi AR, Furutani Y, Jung KH, Kandori H. 2010. Low-temperature FTIR study of gloeobacter rhodopsin: Presence of strongly hydrogen-bonded water and long-range structural protein perturbation upon retinal photoisomerization. Biochemistry 49(15): 3343-3350 https://doi.org/10.1002/lno. 10270

[21] Zhu Y, Xu CH, Huang J, Li GY, Liu XH, et al. 2014. Rapid discrimination of cultivated Codonopsis lanceolata in different ages by FT-IR and 2DCOS-IR. Journal of Molecular Structure 1069: 272-279 https://doi.org/10.1016/j. molstruc.2014.01.069

[22] Szymanska-Chargot M, Zdunek A. 2013. Use of FT-IR spectra and PCA to the bulk characterization of cell wall residues of fruits and vegetables along a fraction process. Food Biophysics 8(1): 29-42 https://doi.org/10.1007/s11483-012-9279-7

[23] Soliman HS, Eid KM, Ali HAM, El-Mansy MAM, Atef SM. 2013. FT-IR spectroscopic analyses of 2-(2-furanylmethylene) propanedinitrile. Spectrochimica Acta Part A: Molecular and Biomolecular Spectroscopy 105: 545-549 https://doi.org/ 10.1016/j.saa.2012.12.051

[24] Prabhu T, Periandy S, Ramalingam S. 2011. FT-IR and FT-Raman investigation, computed vibrational intensity analysis and computed vibrational frequency analysis on m-Xylol using ab-initio HF and DFT calculations. Spectrochimica Acta Part A: Molecular and Biomolecular Spectroscopy 79(5): 948-955 https:// doi.org/ 10.1016/ j. saa.2011.04.001

[25] Selvaraju R, Thiruppathi G, Raja A. 2012. FT-IR spectral studies on certain human urinary stones in the patients of rural area. Spectrochimica Acta Part A: Molecular and Biomolecular Spectroscopy 93: 260-265 https://doi.org/10.1016/ j. saa.2012.03.028

[26] Wiercigroch E, Szafraniec E, Czamara K, Pacia MZ, Majzner K, et al. 2017. Raman and infrared spectroscopy of carbohydrates: A review. Spectrochimica Acta Part A: Molecular and Biomolecular Spectroscopy 185: 317-335 https: // doi.org/ 10.1016/ j. saa.2017.05.045

[27] Linder R, Nispel M, Häber T, Kleinermanns K. 2005. Gas-phase FT-IR-spectra of natural amino acids. Chemical Physics Letters 409(4-6): 260-264 https://doi. org/10. 1016/j.cplett.2005.04.109

[28] Rodríguez FJ, Schlenger P, García-Valverde M. 2016. Monitoring changes in the structure and properties of humic substances following ozonation using UV-Vis, FTIR and 1H NMR techniques. Science of the Total Environment 541: 623-637 https:// doi.org/10.1016/j.scitotenv.2015.09.127

[29] Dikdim JMD, Gong Y, Noumi GB, Sieliechi JM, Zhao X, et al. 2019. Peroxymonosulfate improved photocatalytic degradation of atrazine by activated carbon/graphitic carbon nitride

composite under visible light irradiation. Chemosphere 217: 833-842 https://doi.org/10.1016/j.chemosphere.2018.10.177

[30] Kim HC, Hong JH, Lee S. 2006. Fouling of microfiltration membranes by natural organic matter after coagulation treatment: A comparison of different initial mixing conditions. Journal of Membrane Science 283(1-2): 266-272 https://doi. org/ 10.1016/ j.memsci.2006.06.041

[31] Jaouadi M, Amdouni N, Duclaux L. 2012. Characteristics of natural organic matter extracted from the waters of Medjerda dam (Tunisia). Desalination 305: 64-71 https: //doi.org/10.1016/j.desal.2012.07.008

[32] Ifon BE, Suanon F, Kikia C, Peter PO, Wotto VD, et al. 2024. The interaction between chromophoric dissolved organic matter and xenobiotics (bisphenols and perfluoroalkyl substances) identified by UV-vis absorption and FT-IR spectroscopy. Journal of Molecular Structure 1295: 136762 https://doi.org/ 10. 1016/ j.molstruc. 2023.136762

Table S7 Fluorescence peaks in MPs-DOM and N-DOM under dark and UV conditions.

	Peak	E_x/E_m (nm)	Description	Ref.
MPs-DOM in Dark	Peak B	220/280 - 320	tryptophan-like or phenol-like components	(Mohapatra et al., 2021)
	Peak T	225-300/320-370	bio-labile properties, tryptophan-like components	(Chen et al., 2024)
MPs-DOM under UV	Peak B	220/310	tryptophan-like or phenol-like components	(Mohapatra et al., 2021)
	Peak T	245/440 nm、320/440 nm	bio-labile properties, tryptophan-like components	(Chen et al., 2024)
	Peak C (PET-/PBAT-DOM)	310/430 nm、260/430 nm	terrestrial humic-like, high molecular weight and aromatic humic substances	(Wang et al., 2021)
N-DOM in dark and under UV	Peak A	220-295/420-530	fulvic-like components	(Zhang et al., 2024)
	Peak C	225-365/-375-480	terrestrial humic-like, high molecular weight and aromatic humic substances	(Begum et al., 2023)
	Peak M	290-310/370-420	UVA humic-like materials with a low molecular weight	(Begum et al., 2023)
	Peak T	225-300/320-370	tryptophan-like or phenolic structures	(Su et al., 2015)

References

[1] Mohapatra S, Sharma N, Mohapatra G, Padhye LP, Mukherji S. 2021. Seasonal variation in fluorescence characteristics of dissolved organic matter in wastewater and identification of proteins through HRLC-MS/MS. Journal of Hazardous Materials 413: 125453 https://doi.org/10.1016/j.jhazmat.2021.125453

[2] Chen CZ, Du RJ, Tang J, Wang B, Li F, et al. 2024. Characterization of microplastic-derived dissolved organic matter in freshwater: Effects of light irradiation and polymer types. Environment International 185: 108536 https://doi. org/10.1016/j.envint.2024.108536

[3] Wang XY, Yang QP, Tian SJ, Song FH, Guo F, et al. 2021. Photochemical reactivity of humic substances in an aquatic system revealed by excitation-emission matrix fluorescence. Frontiers in Chemistry 9: 679286 https: //doi.org/10.3389/fchem. 2021. 679286

[4] Zhang H, Chen W, Qi Z, Qian W, Yang L, et al. 2024. Biochar improved the solubility of triclocarban in aqueous environment: Insight into the role of biochar-derived dissolved organic carbon. Chemosphere 351: 141172 https://doi. org/10.1016/j. chemosphere.2024.141172

[5] Begum MS, Park JH, Yang L, Shin KH, Hur J. 2023. Optical and molecular indices of dissolved organic matter for estimating biodegradability and resulting carbon dioxide production in inland waters: A review. Water Research 228: 119362 https://doi. org/ 10.1016/j.watres.2022.119362

[6] Su Y, Chen F, Liu Z. 2015. Comparison of optical properties of chromophoric dissolved organic matter (CDOM) in alpine lakes above or below the tree line: Insights into sources of CDOM. Photochemical & Photobiological Sciences 14(5): 1047-1062 https://doi.org/10.1039/c4pp00478g

Table S8 Major fluorescence peaks and fluorescence regions in MPs-DOM and N-DOM.

	Component	E_{xmax}/E_{mmax}	Description	Ref.
N-DOM in dark	C1-dark	235/430 nm	terrestrial humic-like substances	(Guo et al., 2014)
	C2-dark	365/480 nm	fulvic-like components	(Fischer et al., 2023)
	C3-dark	295/530 nm、235/530 nm	UVA humic-like materials with a low molecular weight	(Lin and Guo, 2020; Rodriguez-Avella et al., 2020)
	C4-dark	225/330 nm	tryptophan-like or phenolic structures	(He et al., 2020; Liu et al., 2024)
MPs-DOM in Dark	C5-dark	220/305 nm	tryptophan-like or phenol-like components	(Lerman et al., 2013; Romero et al., 2017)
	C6-dark	270/320 nm	bio-labile properties, tryptophan-like components	(Liu et al., 2022)
N-DOM under UV	C1-UV	330/440 nm、225/440 nm	fulvic-like components	(Maqbool et al., 2018)
	C2-UV	235/420 nm	terrestrial humic-like, high molecular weight and aromatic humic substances	(Wang et al., 2022)
	C3-UV	270/490 nm	UVA humic-like materials with a low molecular weight	(Zhang et al., 2023)
MPs-DOM under UV	C4-UV	220/310 nm	tryptophan-like or phenol-like components	(Derrien et al., 2019)
	C5-UV	245/440 nm、320/440 nm	bio-labile properties, tryptophan-like components	(Gao et al., 2018)
	C6-UV	310/430 nm、260/430 nm	terrestrial humic-like, high molecular weight and aromatic humic substances	(Wang et al., 2022; Wang et al., 2020)

References

[1] Guo J, Liu H, Liu JH, Wang LY. 2014. Ultrafiltration performance of EfOM and NOM under different MWCO membranes: Comparison with fluorescence spectroscopy and gel filtration chromatography. Desalination 344: 129-136 https: //doi. org/10.1016/j.desal.2014.03.006

[2] Fischer SJ, Fegel TS, Wilkerson PJ, Rivera L, Rhoades CC, et al. 2023. Fluorescence and absorbance indices for dissolved organic matter from wildfire ash and burned watersheds. ACS ES&T Water 3(8): 2199-2209 https://doi.org/ 10.1021/ acsestwater. 3c00017

[3] Lin H, Guo L. 2020. Variations in colloidal DOM composition with molecular weight within individual water samples as characterized by flow field-flow fractionation and EEM-PARAFAC analysis. Environmental Science & Technology 54(3): 1657-1667

https://doi.org/10.1021/acs.est.9b07123

[4] Rodriguez-Avella KA, Baraer M, Mark B, McKenzie J, Somers L. 2020. Comparing the performance of three methods to assess DOM dynamics within two distinct glacierized watersheds of the tropical Andes. Environmental Pollution 265: 115052 https://doi.org/10.1016/j.envpol.2020.115052

[5] He XS, Zhang YL, Liu ZH, Wei D, Liang G, et al. 2020. Interaction and coexistence characteristics of dissolved organic matter with toxic metals and pesticides in shallow groundwater. Environmental Pollution 258: 113736 https: //doi.org/10.1016/j.envpol. 2019.113736

[6] Liu ZH, Liu JM, Zhu PP, Ma Y. 2024. Interaction and coexistence characteristics of dissolved organic matter and toxic metals with per- and polyfluoroalkyl substances in landfill leachate. Environmental Research 260: 119680 https://doi. org/10.1016/j. envres.2024.119680

[7] Lerman I, Chen Y, Xing B, Chefetz B. 2013. Adsorption of carbamazepine by carbon nanotubes: Effects of DOM introduction and competition with phenanthrene and bisphenol A. Environmental Pollution 182: 169-176 https://doi. org/10.1016/ j.envpol. 2013.07.010

[8] Romero CM, Engel RE, D'Andrilli J, Chen C, Zabinski C, et al. 2017. Bulk optical characterization of dissolved organic matter from semiarid wheat-based cropping systems. Geoderma 306: 40-49 https://doi.org/10.1016/j.geoderma. 2017.06.029

[9] Liu D, Gao H, Yu H, Song Y. 2022. Applying EEM-PARAFAC combined with moving-window 2DCOS and structural equation modeling to characterize binding properties of Cu(II) with DOM from different sources in an urbanized river. Water Research 227: 119317 https://doi.org/10.1016/j.watres.2022.119317

[10] Maqbool T, Bae S, Hur J. 2018. Exploring the complex removal behavior of natural organic matter upon N-doped reduced graphene oxide-activated persulfate via excitation-emission matrix combined with parallel factor analysis and size exclusion chromatography. Chemical Engineering Journal 347: 252-262 https:// doi.org/10. 1016/j.cej.2018.04.121

[11] Wang Y, Zou Y, Yang K, Lin D. 2022. Reciprocal interferences of heavy metal and dissolved organic matter on their immobilizations by modulating the interfacial interactions with nanoscale zero-valent iron. Separation and Purification Technology 298: 121671 https://doi.org/10.1016/j.seppur.2022. 121671

[12] Zhang XH, Bai JH, Zhang ZS, Xie T, Zhang GL, et al. 2023. Plant invasion strengthens the linkages between dissolved organic matter composition and the microbial community in coastal wetland soils. Catena 232: 107449 https://doi. org/ 10. 1016/j.catena.2023.107449

[13] Derrien M, Shin KH, Hur J. 2019. Biodegradation-induced signatures in sediment pore water dissolved organic matter: Implications from artificial sediments composed of two contrasting sources. Science of the Total Environment 694: 133714 https:// doi. org/10.1016/j.scitotenv.2019.133714

[14] Gao L, Zhou Z, Reyes AV, Guo L. 2018. Yields and characterization of dissolved organic matter from different aged soils in Northern Alaska. Journal of Geophysical Research: Biogeosciences 123(7): 2035-2052 https://doi.org/10. 1029/2018jg004408

[15] Wang YL, Yang K, Lin DH. 2020. Nanoparticulate zero valent iron interaction with dissolved organic matter impacts iron transformation and organic carbon stability. Environmental Science: Nano 7(6): 1818-1830 https://doi.org/ 10.1039/ d0en00197j

Table S9 Number of intermediate molecular formulae and FT-ICR MS molecular parameters for MPs-DOM and N-DOM.

	PE-DOM				PET-DOM				PBAT-DOM				PLA-DOM				N-DOM			
	dark	6 h	48 h	96 h	dark	6 h	48 h	96 h	dark	6 h	48 h	96 h	dark	6 h	48 h	96 h	dark	6 h	48 h	96 h
formulas	2551	3287	4661	5375	2041	2593	4269	6523	1464	2592	2954	4131	2200	3597	2247	1598	6156	6745	7328	8153
m/z_{wa}	354.17	390.84	423.66	423.86	335.80	447.95	461.65	471.77	393.57	518.63	548.25	480.22	363.23	503.17	494.12	463.41	491.75	454.07	462.09	459.34
H/C_{wa}	1.41	1.30	1.35	1.40	1.47	1.47	1.26	1.20	1.41	1.36	1.31	1.40	1.50	1.41	1.40	1.38	0.97	0.97	0.98	1.01
O/C_{wa}	0.51	0.49	0.52	0.5	0.52	0.40	0.52	0.59	0.46	0.45	0.47	0.52	0.53	0.50	0.57	0.72	0.61	0.56	0.55	0.54
DBE_{wa}	6.01	6.52	7.29	7.26	5.23	6.59	8.29	9.65	6.78	8.39	9.42	7.67	5.26	7.27	6.94	6.76	12.20	11.81	11.96	11.57
$AI_{mod, wa}$	0.13	0.14	0.08	0.11	0.09	0.09	0.16	0.21	0.15	0.14	0.17	0.12	0.05	0.06	0.03	0.002	0.37	0.41	0.40	0.38
$NOSC_{wa}$	-0.35	-0.35	-0.31	-0.36	-0.39	-0.72	-0.26	-0.02	-0.50	-0.54	-0.45	-0.41	-0.40	-0.48	-0.32	0.005	-0.29	0.17	0.16	0.11
MLB_L	0.44	0.30	0.40	0.41	0.52	0.49	0.27	0.18	0.39	0.38	0.30	0.23	0.54	0.40	0.35	0.31	0.04	0.05	0.06	0.08
CHO (%)	57.78	64.74	46.49	57.86	52.92	61.32	56.65	71.58	81.56	87.35	93.54	94.09	55.50	72	77.22	93.93	49.89	61.35	60.21	55.46
CHON (%)	37.08	17.77	38.00	33.62	41.30	14.57	10.37	28.22	17.28	2.43	0.71	5.91	37.27	6.12	5.87	2.94	28.54	26.36	26.24	27.23
CHONS (%)	0.67	0.33	2.42	1.99	0.00	0.47	2.82	0.00	0.00	0.00	0.00	0.00	0.73	0.00	0.00	0.00	4.27	1.76	1.94	2.44
CHOS (%)	4.47	17.16	13.09	6.53	5.78	23.64	30.16	0.20	1.16	10.22	5.75	0.00	6.50	21.88	16.91	3.13	17.30	10.53	11.61	14.87
CAS-like (%)	2.38	5.45	5.15	1.48	1.55	3.63	0.62	2.74	0.26	0.31	0.54	0.19	0.91	0.75	0.62	0.00	11.83	15.91	16.48	15.53
Lignin-like (%)	45.10	55.86	47.76	49.77	39.78	57.32	51.29	58.81	55.47	66.82	71.23	51.08	38.33	49.57	44.24	26.91	54.69	60.55	61.07	62.20
Protein-like (%)	27.49	20.51	28.71	30.19	32.39	20.31	31.01	22.95	24.14	21.60	18.31	14.64	34.64	28.80	26.66	14.46	3.07	3.34	4.35	6.53
HydroC-like (%)	8.75	3.68	6.63	3.08	10.45	2.88	1.23	3.82	5.57	1.08	0.88	6.83	10.82	4.03	4.81	16.02	0.66	0.19	0.29	0.47
Lipid-like (%)	6.33	6.24	5.41	8.15	7.49	4.43	17.28	1.69	7.70	7.72	4.37	2.04	6.43	7.34	3.25	0.69	0.44	1.14	1.15	1.29
UnsatHydroC-like (%)	0.04	0.06	0.15	0.05	0.00	0.00	0.00	0.00	0.00	0.00	0.00	0.02	0.00	0.08	0.00	0.00	0.00	0.00	0.00	0.00
Tannin-like (%)	9.92	11.20	9.48	11.11	8.33	14.62	3.43	12.16	6.86	6.87	7.99	29.29	8.87	13.87	25.68	46.62	29.31	19.11	17.14	14.94

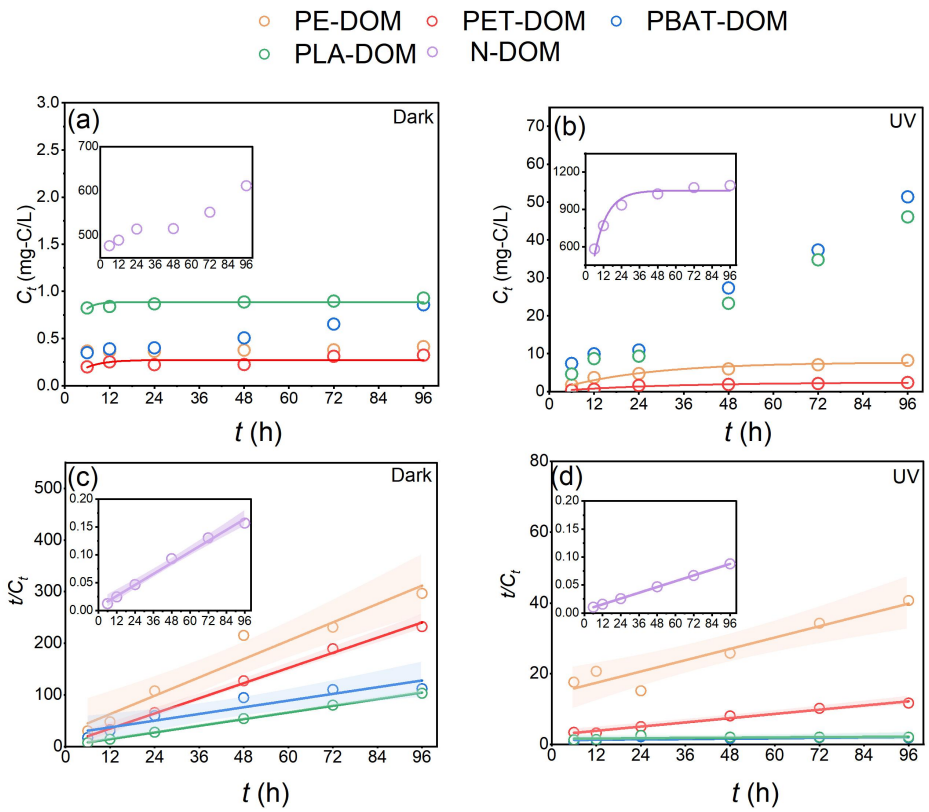

Fig. S1 Derivation of MPs-DOM and N-DOM dissolved organic carbon under dark and UV conditions. (**a, b**) First-order; (**c, d**) Second-order.

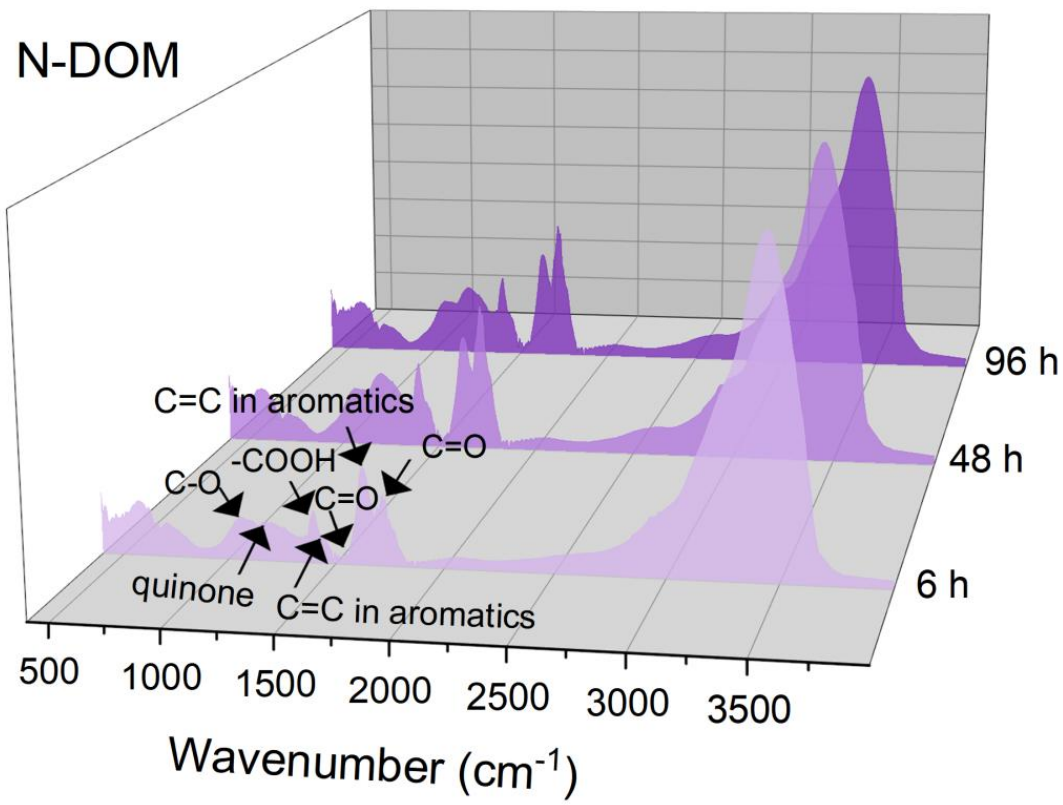

Fig. S2 FT-IR of N-DOM during UV derivation.

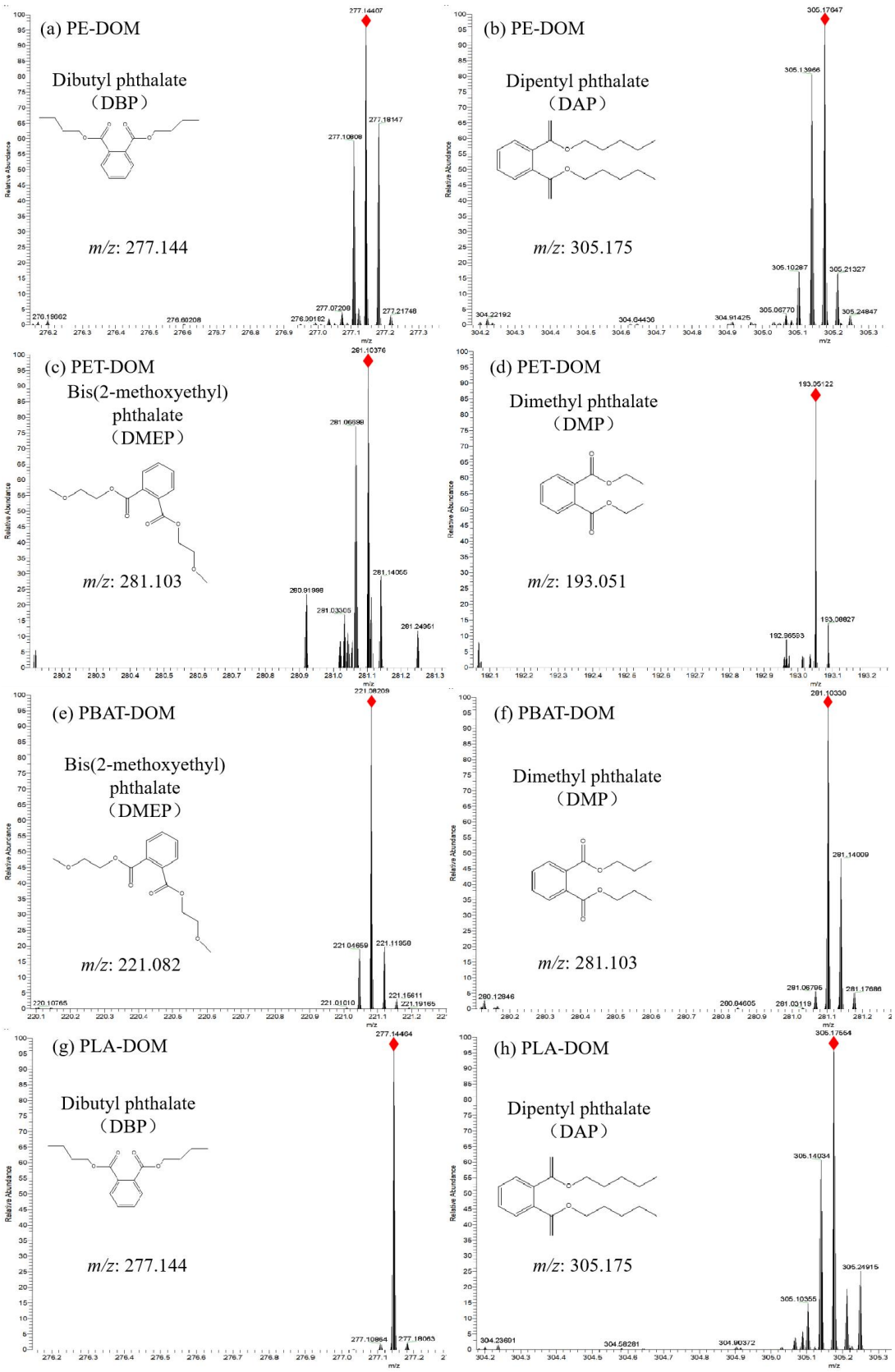

Fig. S3 HPLC-MS/MS spectra of MPs-DOM.

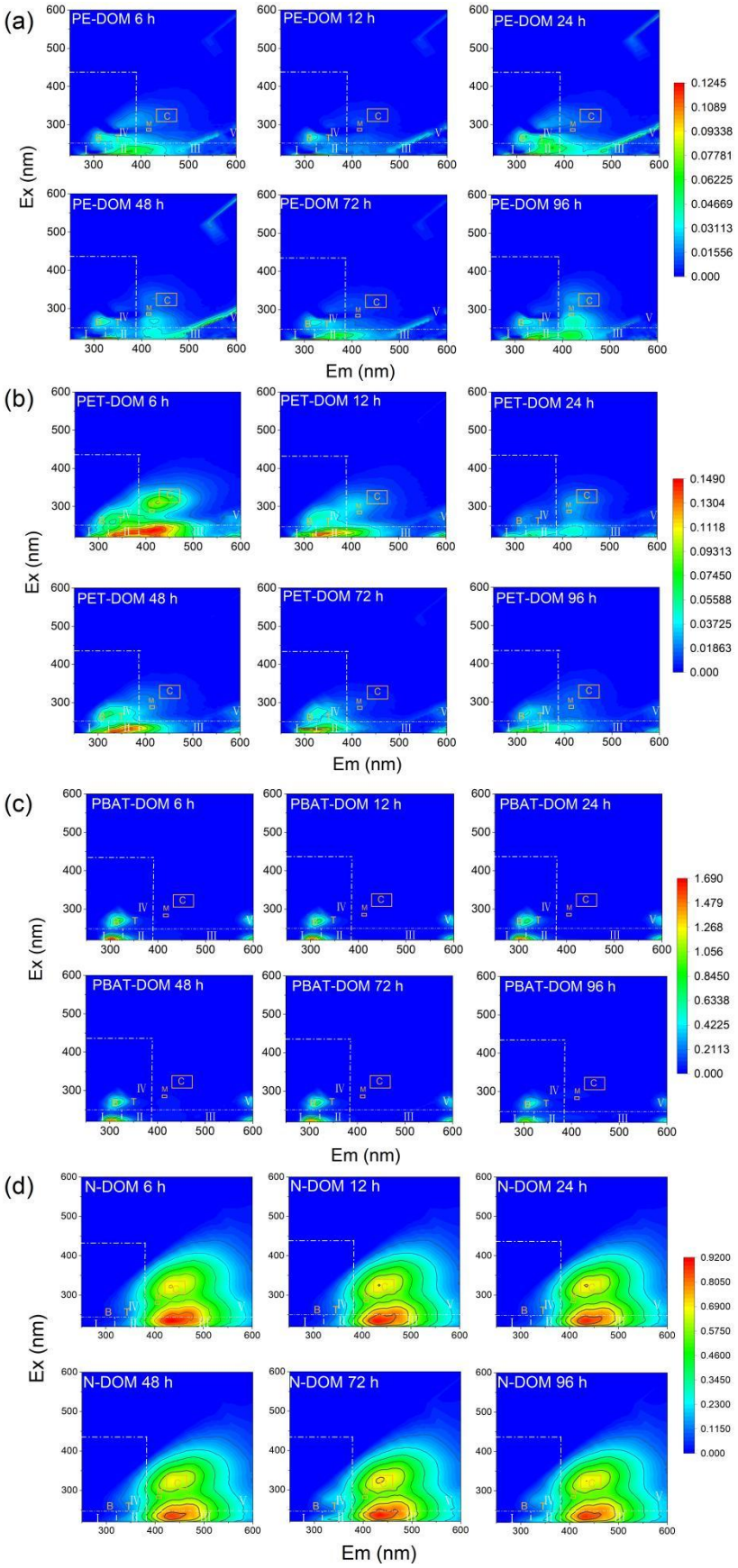

Fig. S4 EEM of MPs-DOM and N-DOM under dark conditions.

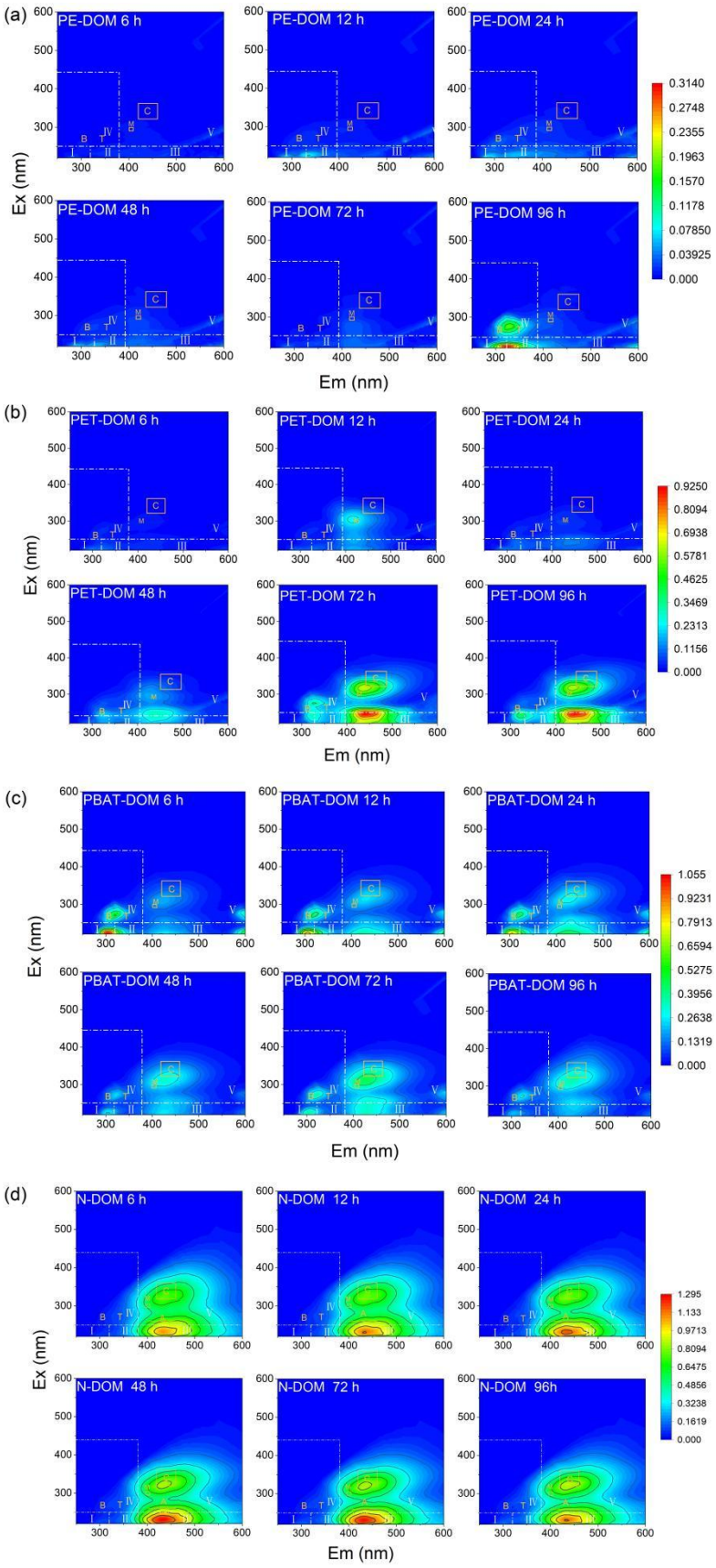

Fig. S5 EEM of MPs-DOM and N-DOM under UV conditions.

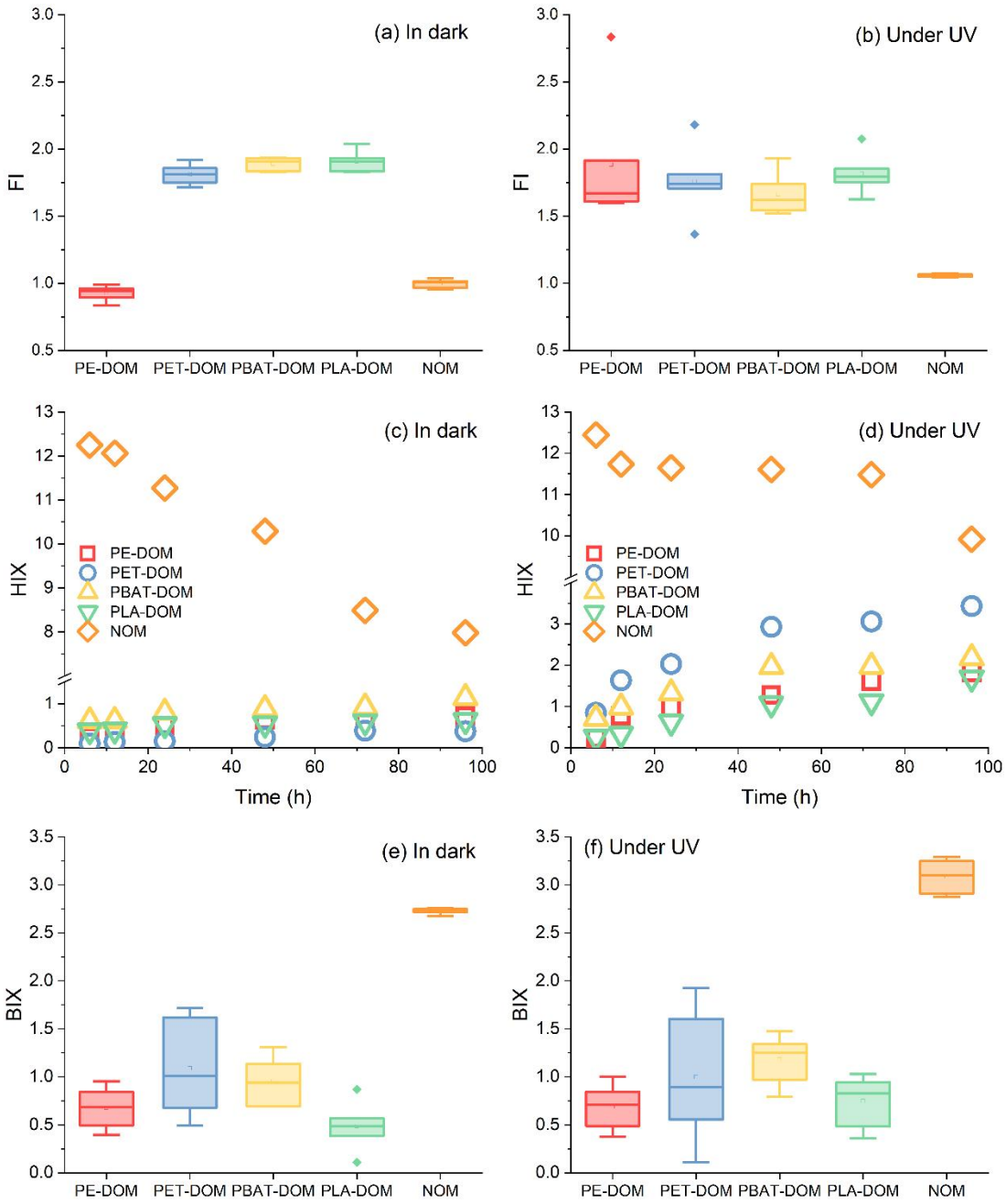

Fig. S6 FI, HIX, and BIX in the derivation processes of MPs-DOM and N-DOM

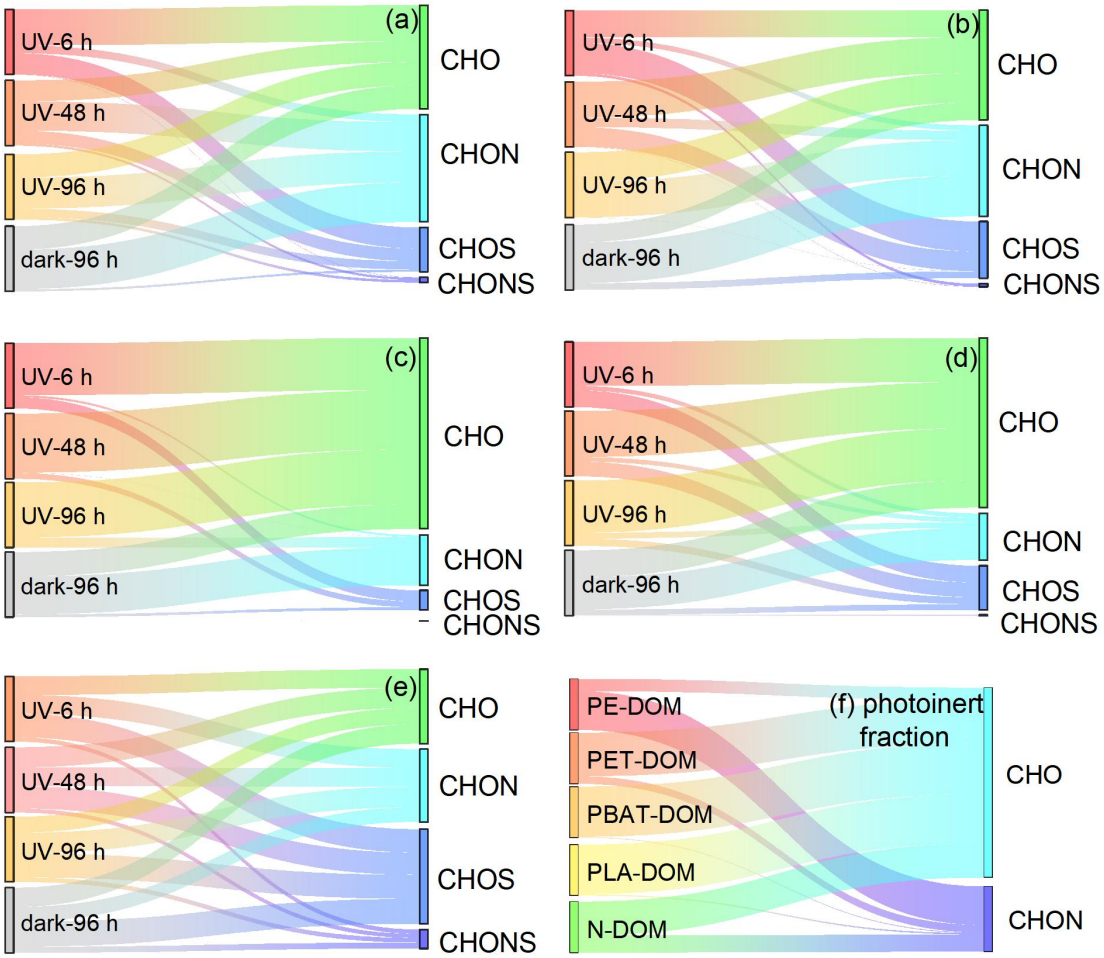

Fig. S7 Changes in molecular composition during derivation.

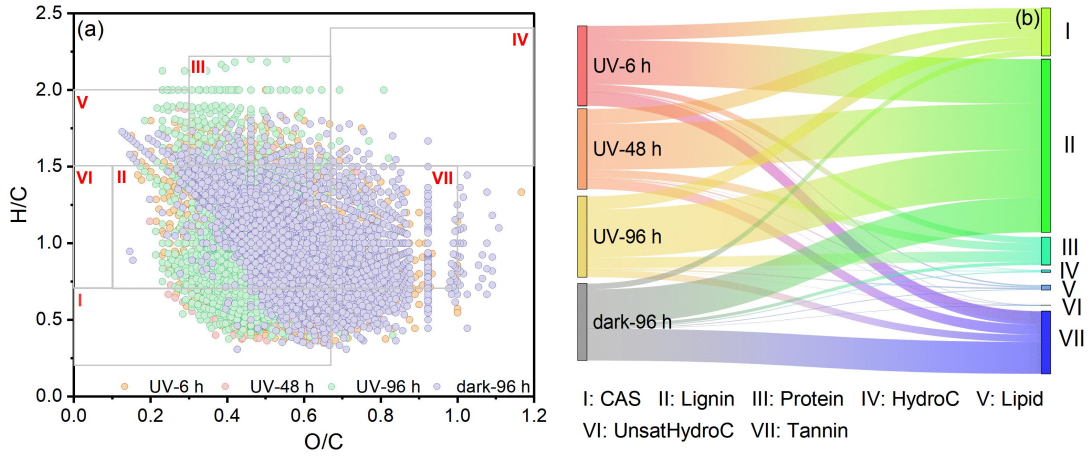

Fig. S8 (**a**) VK diagram of N-DOM during UV derivation processes; (**b**) distribution of typical compound components of N-DOM during UV derivation processes.